Adsorption of H_2O on a Single-Crystal α-Al_2O_3(0001) Surface

J. W. Elam,[†,‡] C. E. Nelson,[†,‡] M. A. Cameron,[†] M. A. Tolbert,[†,‡] and S. M. George*[,†]

Department of Chemistry and Biochemistry and CIRES, University of Colorado, Boulder, Colorado 80309-0215

Received: February 11, 1998; In Final Form: June 14, 1998

The adsorption of H_2O on a single-crystal α-Al_2O_3(0001) surface was examined using laser-induced thermal desorption (LITD) and temperature-programmed desorption (TPD) techniques. α-Al_2O_3(0001) models the surface of Al_2O_3 exhaust particles generated by solid rocket motors that may affect the stratospheric ozone layer. After cleaning and annealing to 1100 K, the α-Al_2O_3(0001) surface displayed a well-defined hexagonal (1 × 1) low-energy electron diffraction (LEED) pattern. Absolute hydroxyl coverages on this α-Al_2O_3(0001) single-crystal surface were determined using H_2O LITD signals. Hydroxylation by the dissociative adsorption of H_2O was differentiated from molecular H_2O adsorption using TPD studies with isotopically labeled $H_2{}^{18}O$. For H_2O dissociative adsorption at 300 K, the initial sticking coefficient was $S \approx 0.1$. The H_2O sticking coefficient decreased nearly exponentially with hydroxyl coverage, and the hydroxyl coverage saturated at $\Theta_{OH} = 0.5 \times 10^{15}$ OH groups/cm^2 after a H_2O exposure of $>10^{10}$ langmuir. For constant H_2O exposures performed at different H_2O pressures, the resulting hydroxyl coverage also increased with H_2O pressure suggesting collisionally activated H_2O adsorption. On the basis of these H_2O adsorption results, α-Al_2O_3 rocket exhaust particles in the stratosphere should be hydroxylated at coverages of $\Theta_{OH} \approx 0.3 \times 10^{15}$ OH groups/cm^2. H_2O adsorption on α-Al_2O_3(0001) was also investigated using a H_2O plasma. Plasma hydroxylation yielded much larger hydroxyl coverages of $\Theta_{OH} = 3.6 \times 10^{15}$ OH groups/cm^2 and destroyed the hexagonal LEED pattern after one plasma exposure. Larger hydroxyl coverages were measured after consecutive H_2O plasma exposures indicating that plasma hydroxylation progressively roughens the α-Al_2O_3(0001) surface.

I. Introduction

The surface chemistry of Al_2O_3 has been studied extensively because alumina is an important industrial catalyst.[1] Much of this work has focused on high surface area γ-Al_2O_3 powders. However, α-Al_2O_3 is widely used as the catalytic support for the industrially important ethylene epoxidation reaction.[2] The sapphire or corundum structure of α-Al_2O_3 is also the most common form of macroscopic-sized Al_2O_3 samples. Unfortunately, very few surface chemistry studies have been conducted on well-defined, single-crystal α-Al_2O_3 surfaces.

Alumina particles are also a major component of exhaust from solid rocket motors. The space shuttle boosters release 276 000 kg of Al_2O_3 into the atmosphere per launch,[3] and approximately 1/3 of these particles are deposited in the stratosphere.[4] Heterogeneous processes on the surfaces of these particles may influence the chemistry of the stratosphere.[5] For instance, these particles may affect stratospheric ozone levels by releasing chlorine from chlorofluorocarbons (CFCs).[6−8] Additionally, Al_2O_3 particles in the stratosphere may catalyze the chlorine activation reaction $ClONO_2 + HCl \rightarrow HNO_3 + Cl_2$.[9,10] The surface reactivity of alumina particles generated by solid rocket motors may be strongly affected by hydroxyl (OH) groups that result from the dissociative adsorption of H_2O.

Solid rocket motor exhaust is composed of both α-Al_2O_3 and γ-Al_2O_3.[11] The α-Al_2O_3(0001) basal plane was chosen to model the α-Al_2O_3 surface because this single-crystal surface is stable and has been well characterized.[12−16] The adsorption of H_2O on α-Al_2O_3 powders[17−19] and single-crystal α-Al_2O_3 $(1\bar{1}02)$[20] have been examined previously using a variety of methods. In this study, the dissociative adsorption of H_2O on α-Al_2O_3(0001) at 300 K was examined using laser-induced thermal desorption (LITD)[21−23] and temperature-programmed desorption (TPD) techniques.[24,25] This study also investigated the hydroxylation of α-Al_2O_3(0001) using a H_2O plasma. The results from this study should help to predict the hydroxyl coverage on the surface of α-Al_2O_3 rocket exhaust particles.

II. Experimental Section

(A) Vacuum Chamber. The details of the ultrahigh vacuum (UHV) apparatus used for these experiments have been given previously.[26−29] Briefly, the main chamber is pumped by both a 400 L/s ion pump and a 5000 L/s cryopump to a base pressure of $2-5 \times 10^{-10}$ Torr. High-pressure exposures and plasma treatments are performed in an internal high-pressure chamber (IHPC) that is in the lower level of the UHV chamber.[30] The sample crystal is coupled to a liquid nitrogen cryostat by a helium thermal switch.[30] This helium thermal switch facilitates a rapid transition between low- and high-temperature experiments.[30] Low-energy electron diffraction (LEED) analysis is performed with a rear view spectrometer (PRI RVL 8-120). The LEED spectrometer is also used in retarding field mode for Auger electron spectroscopy (AES).

(B) Al_2O_3 Surface Preparation and Mounting. Figure 1 shows a schematic of the sample mount. Two α-Al_2O_3(0001) crystals (20 × 15 × 0.75 mm, Crystal Systems) press against a 0.01-mm-thick tantalum foil.[13] These two α-Al_2O_3 crystals are clamped together using 0.25-mm-thick "C"-shaped molyb-

[†] Department of Chemistry and Biochemistry.
[‡] CIRES.

S1089-5647(98)01070-0 CCC: $15.00
Published on Web 08/13/1998

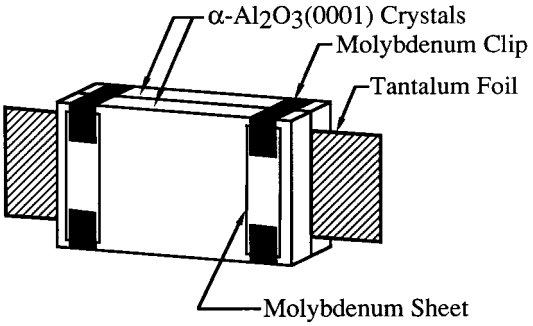

Figure 1. Schematic view of the sample mount.

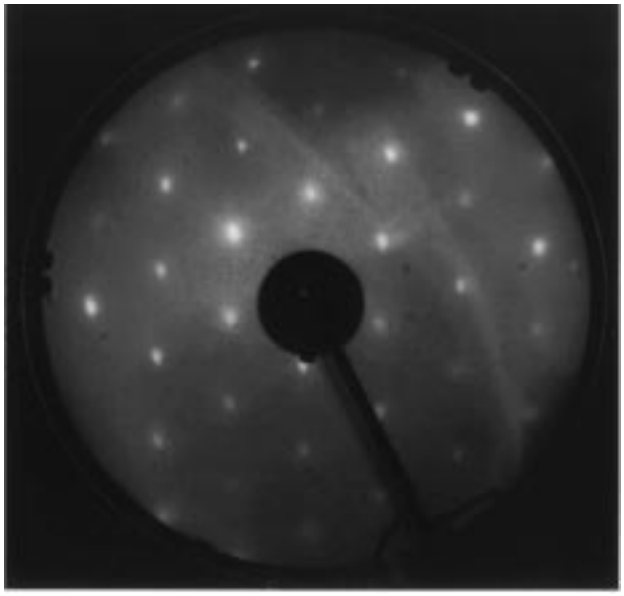

Figure 2. LEED pattern of α-Al_2O_3(0001) recorded at 166 eV.

denum clips. Molybdenum sheets with a 0.25-mm thickness are placed between the clips and the front α-Al_2O_3 crystal to distribute the force of the molybdenum clips.

Prior to mounting, the α-Al_2O_3(0001) crystals are etched in boiling phosphoric acid at 500 K for 3 min.[12] This chemical cleaning treatment is necessary to obtain well-defined LEED patterns. The crystal temperature is measured with a Chromel−Alumel thermocouple attached to the crystal surface using high thermal conductivity ceramic adhesive (Aremco Ceramabond 569.) The crystal can be resistively heated to 1500 K by passing current through the 0.01 mm tantalum foil. The liquid nitrogen cryostat can cool the crystal to 115 K when the helium thermal switch is set for high thermal conductivity.

After they had been wet chemically cleaned and mounted, the α-Al_2O_3(0001) samples showed significant carbon contamination in the AES spectra. The samples were cleaned with a procedure consisting of two oxygen plasma cycles at 0.2 Torr O_2 for 30 s in the IHPC, followed by an 1100 K anneal.[26−28,31] Subsequently, the AES spectra showed only oxygen and aluminum peaks. A small calcium peak appeared at an intensity of several percent after prolonged annealing. This calcium signal was attributed to diffusion from the bulk.

After the samples were cleaned and annealed, a sharp, (1×1) hexagonal LEED pattern was observed using electron beam energies $\geq$107 eV. A picture of this LEED pattern is shown in Figure 2. This LEED pattern is very similar to the results of earlier LEED studies.[12−14,32] In agreement with previous investigations,[12−14,32] a reconstructed LEED pattern emerged when the Al_2O_3 crystal was annealed above 1300 K. To avoid complications arising from the possible different reactivity of the reconstructed α-Al_2O_3(0001) surface, the crystal temperature was kept below 1100 K. All data presented in this paper were taken exclusively on the (1×1) surface.

(C) LITD and TPD. Laser-induced thermal desorption (LITD) experiments[21−23] were performed with a Lumonics 930 pulsed CO_2 TEA laser modified for TEM-00 operation.[27] The 100-ns, 17-mJ laser pulses were focused onto the Al_2O_3 crystal with a f = 38 cm focal length ZnSe lens. The focused laser beam had a diameter of $\sim$450 μm. Laser desorption species were mass analyzed and detected by a UTI 100C quadrupole mass spectrometer with line-of-sight to the α-Al_2O_3(0001) surface. The H_2O LITD signal was measured by monitoring the mass spectrometer signal at $m/e = 18$.

Laser desorption signals from five consecutive laser pulses were added together to yield the total LITD signal from a given spatial location. The CO_2 laser beam was rastered across the surface by use of a pair of mirrors mounted on piezoelectric linear translators. Temperature-programmed desorption (TPD) experiments[24,25] were performed by slowly ramping the α-Al_2O_3 crystal temperature at $\beta = 1$ K/s while monitoring the desorbing species with the UTI 100C quadrupole mass spectrometer.

(D) H_2O Exposures. The H_2O used in this study was high-pressure liquid chromatography (HPLC) grade. This H_2O was purified by several freeze−pump−thaw cycles prior to use. The $H_2{}^{18}O$ (Cambridge Isotope Laboratories, 95−98% pure) was also purified by multiple freeze−pump−thaw cycles. The $H_2{}^{18}O$ content was verified by the mass spectrometer to be >95%. Low H_2O exposures were achieved by backfilling H_2O in the UHV chamber. Intermediate H_2O exposures were obtained using a glass capillary array doser in the UHV chamber. High-pressure H_2O exposures were conducted in the internal high-pressure chamber (IHPC).

Each H_2O plasma exposure was performed in the IHPC with a H_2O pressure of 250 mTorr. The H_2O plasma was created by discharging a Tesla coil through an electrical feedthrough that led to the IHPC. The H_2O plasma discharge times were approximately 30 s. For multiple plasma exposures, the IHPC was evacuated between plasma exposures. After the hydroxyl coverages were measured, the α-Al_2O_3(0001) surface was dehydroxylated by annealing the crystal above 700 K.[29]

(E) H_2O LITD Signal Calibrations. Calibration experiments were performed to convert the H_2O LITD signals into a hydroxyl coverage in OH groups/cm^2. For these calibrations, an ice film was grown on the α-Al_2O_3(0001) crystal at 120 K by H_2O condensation at a known H_2O background pressure. H_2O LITD signals were measured versus time during the H_2O exposures. The H_2O LITD signals from a typical experiment at an H_2O pressure of 1.0×10^{-8} Torr are shown in Figure 3.

Figure 3 yields the rate of increase of the H_2O LITD signal at a given H_2O pressure. The H_2O LITD signal can be calibrated by knowing that the sticking coefficient and condensation coefficient for H_2O on an ice multilayer are both unity for temperatures below 150 K.[33] Consequently, the ice film growth rate (H_2O molecules cm^{-2} s^{-1}) can be determined from the H_2O background pressure. The H_2O LITD signal calibration is obtained when this ice film growth rate is divided by the slope (H_2O LITD signal s^{-1}) of Figure 3.

This H_2O LITD signal calibration relies on the absolute H_2O pressure as measured by a Bayard−Alpert ionization gauge (IG). The ion gauge was calibrated in two ways. First, the ion gauge measurements were compared with concurrent measurements from a Baratron absolute pressure capacitance manometer

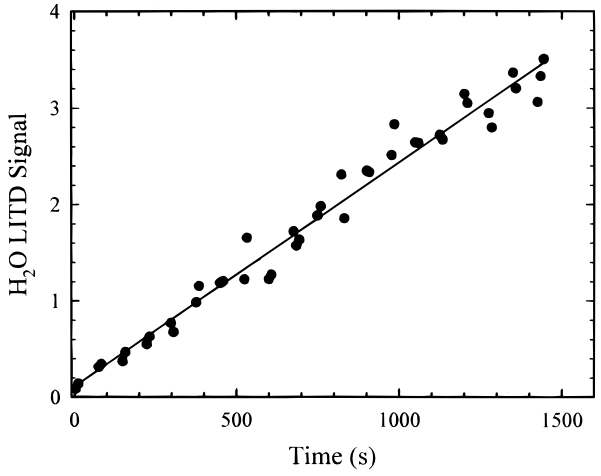

Figure 3. H_2O LITD signal versus time during the growth of an ice multilayer on α-Al_2O_3(0001) at 120 K at a H_2O pressure of 1.0×10^{-8} Torr.

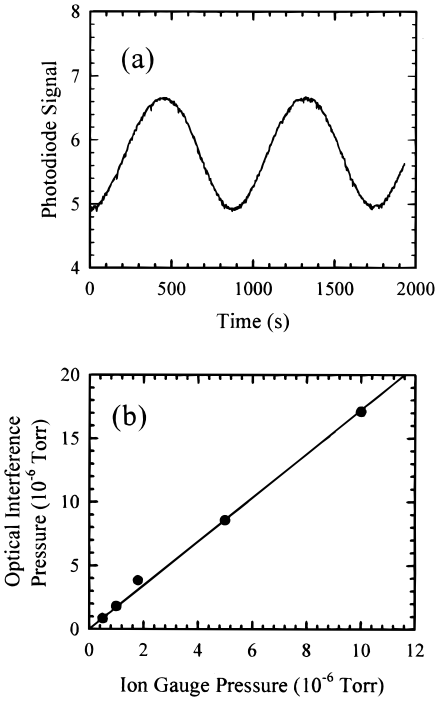

Figure 4. (a) Photodiode signal versus time during the growth of an ice multilayer on α-Al_2O_3(0001) at 120 K at a H_2O pressure of 1.0×10^{-6} Torr as measured by the ion gauge. (b) Comparison between the pressure determined by the optical interference measurements and the ion gauge pressure.

(BAR) for various H_2O pressures between 5×10^{-7} and 1×10^{-3} Torr. The average ratio of these readings was $P_{BAR}/P_{IG} = 2.2$.

The ion gauge was also calibrated using optical interference techniques.[34,35] For these calibrations, a helium−neon laser was reflected from the α-Al_2O_3(0001) surface at near normal incidence. The reflected beam intensity was then measured with a photodiode. Interference between the two beams reflecting from the vacuum−ice and ice−Al_2O_3 interfaces yielded a sinusoidal signal versus H_2O exposure.[34,35] The growth rate was calculated from the period of the signal oscillation.

Figure 4a shows the oscillation in the photodiode signal for a H_2O background pressure of $P_{IG} = 1.0 \times 10^{-6}$ Torr and a surface temperature of 120 K. The density and refractive index of ice have been measured for ice films deposited at different H_2O exposures and substrate temperatures.[34] Consequently, an ice film growth rate can be deduced from the time required for one period of the signal oscillation in Figure 4a. The ice film thickness corresponding to one interference cycle in Figure 4a is $d = 2415$ Å.

Since the condensation coefficient is unity at 120 K,[33] the H_2O pressure above the ice surface during the optical interference (OI) measurements can be derived from kinetic gas theory:

$$P_{OI} = (2RT\lambda\rho/n\upsilon m)(1/t) \quad (1)$$

In this equation, R is the gas constant, T is temperature ($T = 294$ K), λ is the He−Ne wavelength ($\lambda = 6328$ Å), ρ is density ($\rho = 0.93$ g/cm^3), n is the refractive index ($n = 1.31$), υ is the average molecular velocity ($\upsilon = 588$ m/s), m is atomic weight ($m = 18.02$ g/mol), and t is the period of the cycle. P_{OI} measured by the ice film growth rates is plotted versus P_{IG} in Figure 4b. The slope of this line yields $P_{OI}/P_{IG} = 1.8$. This optical interference calibration and the Baratron calibration indicate that the pressure measured by the Bayard−Alpert ionization gauge is low by factors of 2.2 and 1.8, respectively. Consequently, an average multiplication factor of 2.0 was utilized to correct the pressure measured by the ionization gauge.

To determine the hydroxyl surface coverage, the measured H_2O LITD signal in H_2O molecules/cm^2 can be converted to hydroxyl coverage in OH groups/cm^2. Dehydroxylation occurs via the reaction

$$2AlOH^* \rightarrow AlOAl^* + H_2O(g) \quad (2)$$

where * denotes a surface species. According to the above stoichiometry, each H_2O molecule desorbed from the Al_2O_3 surface arises from two hydroxyl units. Consequently, the hydroxyl coverage, Θ_{OH}, is equal to 2× the calibrated H_2O signal. The uncertainty for this calibration of the H_2O LITD signal is ±20%. This uncertainty results from uncertainty in both the ion gauge correction factor and in the rate of increase of the H_2O LITD signal at a given H_2O pressure (Figure 3).

III. Results

(A) Isotopic Experiments. H_2O may dissociatively adsorb on α-Al_2O_3(0001) or H_2O may remain an intact molecular species. Isotopic experiments were performed to determine if H_2O dissociatively adsorbs. The surface was exposed to either 9.2×10^7 langmuir (1 langmuir = 10^{-6} Torr s) $H_2{}^{16}O$ or 9.2×10^7 langmuir $H_2{}^{18}O$ (>95% pure). With a H_2O pressure of 250 mTorr, this H_2O exposure was determined by H_2O LITD measurements to produce a hydroxyl coverage of $\Theta_{OH} = 0.32 \times 10^{15}$ OH groups/cm^2. TPD experiments were then performed at $\beta = 1$ K/s by monitoring both $H_2{}^{16}O$ ($m/e = 18$) and $H_2{}^{18}O$ ($m/e = 20$). The TPD results for these two experiments are shown in Figure 5.

The solid circles in Figure 5 identify the $H_2{}^{18}O$ ($m/e = 20$) TPD curve following the 9.2×10^7 langmuir $H_2{}^{18}O$ exposure. The $H_2{}^{18}O$ TPD curve has a single, broad peak with a maximum at 375 K. The solid triangles in Figure 5 designate the corresponding $H_2{}^{16}O$ ($m/e = 18$) TPD curve following the same 9.2×10^7 langmuir $H_2{}^{18}O$ exposure. This $H_2{}^{16}O$ TPD curve displays a single, broad peak with a maximum at 395 K.

The presence of both $H_2{}^{18}O$ and $H_2{}^{16}O$ in the TPD spectra following $H_2{}^{18}O$ exposure indicates that a large fraction of $H_2{}^{18}O$ is dissociatively adsorbed on α-Al_2O_3(0001). Subsequently, ^{16}O from the Al_2O_3 surface and ^{18}O from the dissociatively adsorbed $H_2{}^{18}O$ are incorporated into H_2O during recombinative desorption. The $H_2{}^{18}O$ and $H_2{}^{16}O$ TPD curves have slightly different

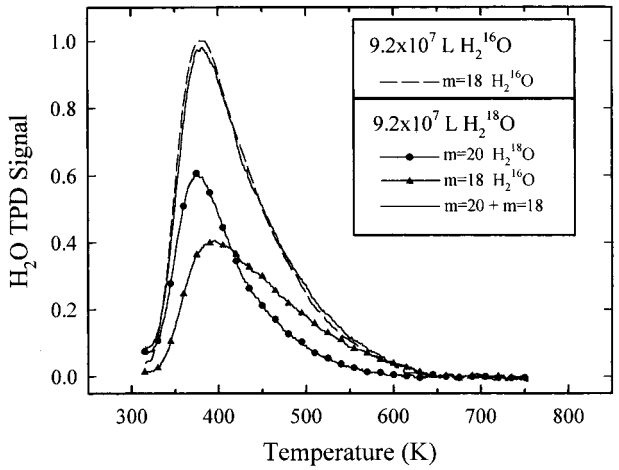

Figure 5. TPD spectra of $H_2{}^{18}O$ ($m/e = 20$, solid circles) and $H_2{}^{16}O$ ($m/e = 18$, solid triangles) following a 9.2×10^7 langmuir $H_2{}^{18}O$ dose at 300 K. The solid line without an identifying symbol shows the sum of the $H_2{}^{18}O$ and $H_2{}^{16}O$ TPD curves following a 9.2×10^7 langmuir $H_2{}^{18}O$ dose. The dashed line shows the $H_2{}^{16}O$ TPD curve following a 9.2×10^7 langmuir $H_2{}^{16}O$ dose.

peak shapes. However, the ratio of the integrated TPD curves is $H_2{}^{16}O$ ($m/e = 18$)/$H_2{}^{18}O$ ($m/e = 20$) = 0.98. The α-Al_2O_3(0001) surface was periodically exposed to a $^{16}O_2$ plasma to maintain the >99% isotopic abundance of ^{16}O in naturally occurring Al_2O_3.

The solid line without an identifying symbol in Figure 5 is the sum of the $H_2{}^{18}O$ and $H_2{}^{16}O$ TPD curves. This sum represents the total H_2O TPD signal following a 9.2×10^7 langmuir $H_2{}^{18}O$ exposure. For comparison, the dashed line is the TPD curve for $H_2{}^{16}O$ ($m/e = 18$) recorded after a 9.2×10^7 langmuir $H_2{}^{16}O$ exposure. The similarity in shape, peak position, and integrated area between the solid line and the dashed line in Figure 5 indicates that the same types of hydroxyl groups are populated during the $H_2{}^{16}O$ and $H_2{}^{18}O$ exposures on α-Al_2O_3(0001).

(B) LEED and AES Measurements. In addition to the measurements performed on the cleaned and annealed α-Al_2O_3(0001) surface, LEED and AES measurements were also performed on an α-Al_2O_3(0001) surface partially hydroxylated at a hydroxyl coverage of $\Theta_{OH} = 0.32 \times 10^{15}$ OH groups/cm^2. The results obtained on this surface were indistinguishable from the LEED and AES results obtained on the clean α-Al_2O_3(0001) surface. However, after exposure to either the LEED or AES electron beam, LITD measurements revealed that the partially hydroxylated surface was completely dehydroxylated.

Dehydroxylation stimulated by electron bombardment on Al_2O_3 has been observed previously.[20,36] In addition, we note that the ~1-mm^2 electron beam could dehydroxylate the entire ~1-cm^2 α-Al_2O_3(0001) surface. This surprising behavior is similar to previously observed phenomena concerning electron-stimulated crystal reconstruction.[12] The mechanism for these collective surface effects is not known.

In separate experiments, the α-Al_2O_3(0001) crystal was annealed to 1300 K and subsequently analyzed by LEED. The resulting LEED pattern resembled the previously observed [$31^{1/2} \times 31^{1/2}$]$R \pm 9°$ reconstruction.[12−14,32] In these earlier LEED studies, some α-Al_2O_3(0001) samples that had not been chemically etched displayed this surface reconstruction after heating to 1000−1200 K. However, most of the chemically etched α-Al_2O_3(0001) surfaces displayed this reconstructed surface pattern only after heating to 1300−1500 K.[12−14,32]

(C) Thermal Hydroxylation. Figure 6 shows the hydroxyl coverage versus H_2O exposure monitored by the H_2O LITD signals. These experiments were performed at room temperature for exposures from 10^0 to 10^{10} langmuir. The H_2O pressures were varied widely to achieve this large range of H_2O exposures. For typical exposure times of 1−15 min, the H_2O pressures varied from 10^{-9} to 13 Torr. After a steep rise in the hydroxyl coverage at low H_2O exposures, the hydroxyl coverage levels off at H_2O exposures $> 0.3 \times 10^9$ langmuir. The α-Al_2O_3(0001) surface reactivity saturates at a hydroxyl coverage of $\Theta_{OH} \approx 0.5 \times 10^{15}$ OH groups/cm^2.

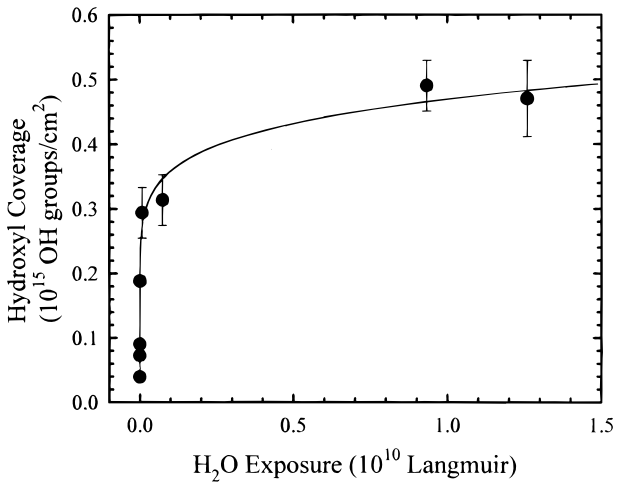

Figure 6. Hydroxyl coverage measured on α-Al_2O_3(0001) versus H_2O exposure at 300 K. The hydroxyl coverage saturates at $\Theta_{OH} = 0.5 \times 10^{15}$ OH groups/cm^2. The solid line is intended only to guide the eye.

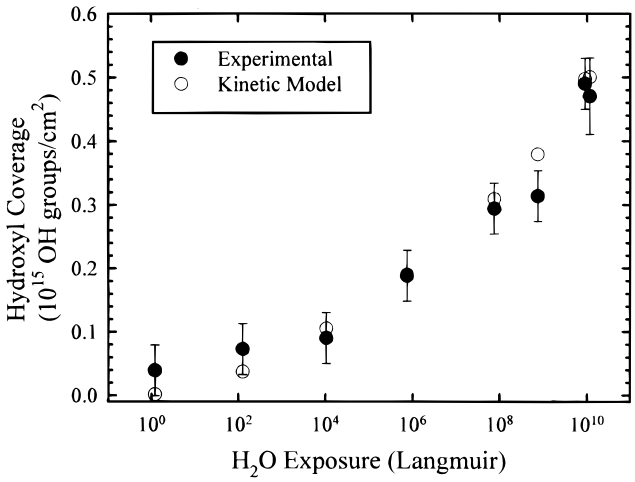

Figure 7. The solid circles display the hydroxyl coverage measured on α-Al_2O_3(0001) versus H_2O exposure at 300 K where H_2O exposure is plotted on a logarithmic scale. The open circles show the hydroxyl coverages predicted by the kinetic model.

The solid circles of Figure 7 show the hydroxyl coverage versus H_2O exposure plotted on a logarithmic H_2O exposure scale. The hydroxyl coverage shows a near logarithmic dependence on H_2O exposure. The open circles in Figure 7 result from a kinetic model of the hydroxylation process that is described in section IV(B). The H_2O pressures and exposure times modeled by the open circles were identical to those used in the corresponding LITD experiments.

Figure 8 shows the data of Figure 6 expressed as sticking coefficient (S) versus hydroxyl coverage (Θ_{OH}). The H_2O sticking coefficient is defined as:

$$S = (d\Theta_{OH}/dt)(1/\phi_{H_2O}) \qquad (3)$$

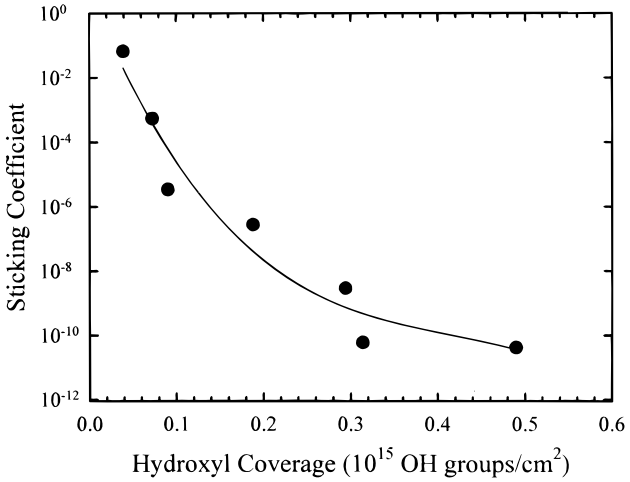

Figure 8. Sticking coefficient for H_2O on α-Al_2O_3(0001) versus hydroxyl coverage at 300 K. The solid line is intended only to guide the eye.

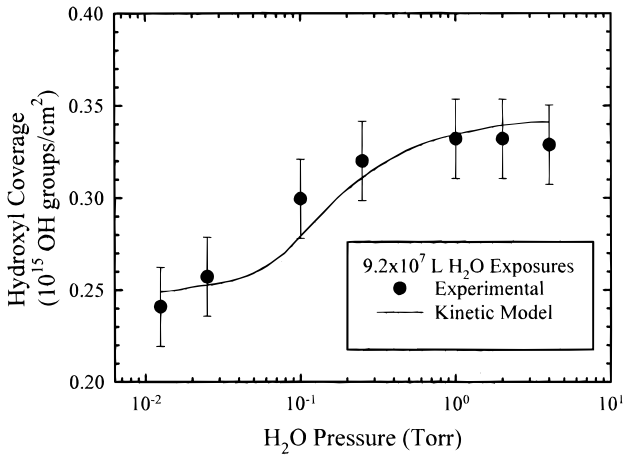

Figure 9. Hydroxyl coverage on α-Al_2O_3(0001) versus H_2O pressure for a total H_2O exposure of 9.2×10^7 langmuir.

where Θ_{OH} is the hydroxyl coverage and ϕ_{H_2O} is the flux of H_2O molecules onto the α-Al_2O_3(0001) surface. The ordinate on Figure 8 is logarithmic. The H_2O sticking coefficient S decreases nearly exponentially with hydroxyl coverage from $S \approx 10^{-1}$ at very low hydroxyl coverage to $S \approx 10^{-11}$ at a saturation hydroxyl coverage of $\Theta_{OH} = 0.5 \times 10^{15}$ OH groups/cm^2.

A wide range of H_2O pressures was employed to obtain the hydroxyl coverage versus H_2O exposure data shown in Figures 6 and 7. To determine the possible pressure dependence of the H_2O adsorption, additional experiments were performed at a constant H_2O exposure of 9.2×10^7 langmuir using different H_2O pressures ranging from 0.0125 to 4 Torr. The results of these investigations are shown as the solid circles in Figure 9.

If the H_2O sticking coefficient is independent of H_2O pressure, an identical hydroxyl coverage should result from equivalent H_2O exposures. For a H_2O exposure of 9.2×10^7 langmuir, Figure 9 reveals that the hydroxyl coverage increases slightly with H_2O pressure. At H_2O pressures exceeding 1 Torr, the hydroxyl coverage levels off and becomes independent of pressure. The solid line in Figure 9 is derived from the kinetic model for hydroxylation described in section IV(B) for H_2O exposures of 9.2×10^7 langmuir at different H_2O pressures.

(D) Plasma Hydroxylation. Figure 10 shows the hydroxyl coverage on α-Al_2O_3(0001) after different numbers of H_2O plasma cycles. The hydroxyl coverages were measured by the

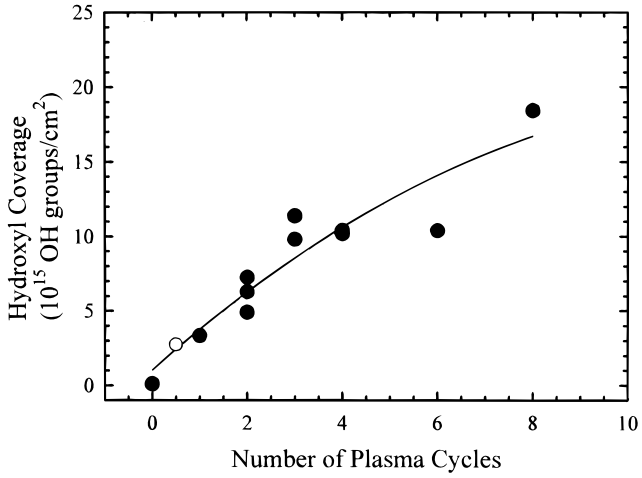

Figure 10. Hydroxyl coverage on α-Al_2O_3(0001) versus number of H_2O plasma cycles.

H_2O LITD signals. The solid circles result from experiments where a clean, dehydroxylated α-Al_2O_3(0001) surface exhibiting a sharp (1×1) LEED pattern was exposed to various numbers of 30-s H_2O plasma cycles. The open circle at 0.5 plasma cycle resulted from one 15-s plasma cycle.

The hydroxyl coverages produced by the H_2O plasma exposures in Figure 10 are much greater than the hydroxyl coverages resulting from thermal hydroxylation shown in Figure 6. Figure 10 shows no sign of saturation of the hydroxyl coverage. Some evidence of a slightly slower growth in the hydroxyl coverage versus number of H_2O plasma cycles is apparent near six to eight plasma cycles.

In addition to the much larger hydroxyl coverages, no LEED pattern was observed after one H_2O plasma cycle. Prolonged annealing at 1100 K was needed to restore the sharp (1×1) LEED pattern. The annealing time required to restore the LEED pattern increased with the number of previous H_2O plasma cycles.

The H_2O plasma treatment also enhanced the H_2O dissociative adsorption on the α-Al_2O_3 surface. A clean, dehydroxylated α-Al_2O_3(0001) surface exhibiting a sharp (1×1) LEED pattern yielded a hydroxyl coverage of $\Theta_{OH} = 0.32 \times 10^{15}$ OH groups/cm^2 after a thermal H_2O exposure of 9.2×10^7 langmuir using a H_2O pressure of 0.25 Torr. Subsequently, the Al_2O_3 surface was dehydroxylated by annealing to 700 K, subjected to eight H_2O plasma cycles, and again annealed to 700 K to remove the hydroxyl groups deposited by the plasma. This Al_2O_3 surface was again exposed to 9.2×10^7 langmuir H_2O, and the resulting hydroxyl coverage was $\Theta_{OH} = 0.50 \times 10^{15}$ OH groups/cm^2.

IV. Discussion

(A) Isotopic Evidence for Surface Hydroxylation. The initial fraction of ^{18}O present on the α-Al_2O_3(0001) surface attributed to natural abundance is only 2×10^{-3}. Consequently, the expected ratio of the integrated mass spectrometric TPD curves for $H_2{}^{16}O/H_2{}^{18}O$ resulting from dissociative adsorption of $H_2{}^{18}O$ and complete scrambling is $[m/e = 18/m/e = 20] = 1.0$. In contrast, the $H_2{}^{16}O/H_2{}^{18}O$ ratio expected from associative molecular adsorption of $H_2{}^{18}O$ is $[m/e = 18/m/e = 20] = 0$.

The ratio of the integrated desorption areas in Figure 5 is $[m/e = 18/m/e = 20] = 0.98$ following an $H_2{}^{18}O$ exposure of 9.2×10^7 langmuir using an $H_2{}^{18}O$ pressure of 0.25 Torr. The ratio of 0.98 provides clear evidence that scrambling has

occurred between the isotopically labeled ^{18}O atoms in $H_2{}^{18}O$ and the ^{16}O atoms initially present on the α-Al_2O_3 surface. This ratio indicates that $H_2{}^{18}O$ has dissociatively adsorbed to form surface hydroxyl groups.

In agreement with the dissociative adsorption of $H_2{}^{18}O$, no evidence is observed for molecular H_2O on α-Al_2O_3 at 300 K in high-resolution electron energy loss spectroscopy (HREELS)[37−39] or in X-ray photoelectron spectroscopy studies.[37] This method of differentiating dissociative adsorption from associative adsorption using isotopic TPD experiments has been used previously to examine H_2O adsorption on MgO(100) at 100 K.[40] In the previous study, the ratio of the integrated desorption areas was $[m/e = 18/m/e = 20] \approx 0$. This ratio indicates that either H_2O adsorbs associatively on MgO(100) or that dissociative adsorption of $H_2{}^{18}O$ does not incorporate ^{16}O from the surface upon recombinative desorption.

Figure 5 shows that the $H_2{}^{18}O$ TPD curve peaks at 375 K. In contrast, the $H_2{}^{16}O$ TPD curve peaks at 395 K following an $H_2{}^{18}O$ exposure. A mass-dependent explanation for this difference in TPD peak positions may be ruled out for two reasons. In contrast to observations, the kinetic isotope effect would cause the more massive $H_2{}^{18}O$ to desorb at a higher temperature than $H_2{}^{16}O$. The composite H_2O TPD curve following an $H_2{}^{18}O$ exposure, i.e., the solid line in Figure 5 for $m/e = 20 + m/e = 18$, is also identical to the $H_2{}^{16}O$ TPD curve following an equivalent $H_2{}^{16}O$ exposure. This behavior indicates that the range and distribution of desorption activation energies is independent of the oxygen isotopic species.

The difference in $H_2{}^{18}O$ and $H_2{}^{16}O$ TPD peak temperatures and the equal integrated desorption areas for $H_2{}^{18}O$ and $H_2{}^{16}O$ is somewhat difficult to reconcile. If $H_2{}^{18}O$ dissociatively adsorbs and then desorbs first, the $H_2{}^{18}O$ integrated desorption area should be larger than the $H_2{}^{16}O$ integrated desorption area. The equal integrated desorption areas argue that the $H_2{}^{18}O$ that desorbs first must desorb by the recombination of only $^{18}OH^*$ hydroxyl groups:

$$Al^{18}OH^* + Al^{18}OH^* \rightarrow Al\text{-}^{18}O\text{-}Al^* + H_2{}^{18}O(g)$$

The $H_2{}^{16}O$ that desorbs later would then desorb by the recombination of only $^{16}OH^*$ hydroxyl groups.

This desorption sequence may occur according to the following scenario if the $H_2{}^{18}O$ that dissociatively adsorbs deposits $^{18}OH^*$ surface species on the aluminum atoms on the topmost layer of the α-Al_2O_3(0001) surface.[41−43] The additional $^{16}OH^*$ surface species formed by $H_2{}^{18}O$ dissociative adsorption may establish hydroxyl groups on the ^{16}O atoms in the second atomic layer on the α-Al_2O_3(0001) surface. If the $^{18}OH^*$ species in the topmost layer preferentially desorb with themselves at lower temperatures, $H_2{}^{18}O$ can be desorbed without removing $^{16}OH^*$. These $^{16}OH^*$ species can then desorb as $H_2{}^{16}O$ at higher temperatures and maintain equal desorption areas for $H_2{}^{18}O$ and $H_2{}^{16}O$.

(B) Kinetic Scheme for H_2O Dissociative Adsorption. Figure 8 displays a strong dependence of the H_2O sticking coefficient, S, on hydroxyl coverage. Figure 9 shows that the hydroxyl coverage resulting from a given H_2O exposure depends on the pressure of the H_2O exposure. The high initial reactivity of H_2O on α-Al_2O_3(0001) at low hydroxyl coverage has been observed previously in HREELS studies.[36] In addition, the rapid decrease of the H_2O dissociative adsorption rate versus hydroxyl coverage resembles the behavior for H_2O adsorption on α-Al_2O_3 measured with differential calorimetry.[19] Although there have been no previous observations of pressure-dependent H_2O adsorption on α-Al_2O_3, a collision-induced hydroxylation mechanism on α-Al_2O_3(0001) has been invoked in molecular dynamics simulations.[42] Additionally, hydroxylation of α-Al_2O_3(0001) was found to be catalyzed by a second H_2O molecule in recent ab initio calculations.[43]

To explain the dependence of the sticking coefficient on hydroxyl coverage (Figure 8) and the pressure dependence of the hydroxyl coverage after constant exposures at different H_2O pressures (Figure 9), the following kinetic model is postulated:

$$H_2O(g) + \text{Al-O-Al}^* \underset{k_{-1}}{\overset{k_1(\Theta)}{\rightleftharpoons}} \text{Al-O-Al}^*(H_2O) \quad (4)$$

$$H_2O(g) + \text{Al-O-Al}^*(H_2O) \xrightarrow{k_2} 2\text{AlOH}^* + H_2O(g) \quad (5)$$

$$\text{Al-O-Al}^*(H_2O) \xrightarrow{k_3} 2\text{AlOH}^* \quad (6)$$

In this kinetic model, $H_2O(g)$ is a gas phase water molecule, Al-O-Al* represents an empty adsorption site on the Al_2O_3 surface, Al-O-Al*(H_2O) is a H_2O precursor, AlOH* represents a surface hydroxyl group, Θ is the hydroxyl coverage, $\Theta = [\text{AlOH}^*]$, and $k_1(\Theta)$ is a function of Θ.

A separate publication[29] will show that the H_2O desorption kinetics from α-Al_2O_3(0001) are independent of hydroxyl coverage. To reconcile this behavior with the strongly coverage-dependent H_2O sticking coefficient, H_2O adsorption is proposed to occur through the Al-O-Al*(H_2O) precursor state in eq 4. An exponential decrease in $k_1(\Theta)$ with hydroxyl coverage reproduces the near logarithmic dependence of sticking coefficient on hydroxyl coverage (Figure 8). The pressure dependence of eq 5 generates an increase in hydroxyl coverage with pressure at constant total exposure (Figure 9). Saturation of the precursor in eq 4 produces a corresponding saturation of hydroxyl coverage after H_2O exposures at high H_2O pressures (Figure 9). Finally, a pressure-independent pathway for hydroxyl formation given by eq 6 models the surface reactivity at low H_2O pressures.

Equations 4−6 were numerically integrated to determine the final hydroxyl coverage resulting from a given H_2O exposure and H_2O pressure. At the start of each simulation, $\Theta = 0$, Al-O-Al* $= 0.25 \times 10^{15}$ cm^{-2}, and $H_2O(g)$ is the pressure in Torr. The following values for the kinetic parameters were found to model the data well: $k_1(\Theta) = 4.7 \times 10^3[\exp(-6.1 \times 10^{-14}(\Theta)) + 10^{-7}]$, $k_{-1} = 10$, $k_2 = 376$, and $k_3 = 4$. These parameters were used for the kinetic model fits in Figures 7 and 9. Although the kinetic model fits the data very well, the kinetic scheme described by eqs 4−6 may not be unique. In addition, the kinetic parameters were determined empirically and other combinations of parameters may yield similar fits.

Some possible physical interpretations for $k_1(\Theta)$ include surface defects, surface relaxation, repulsive interactions, and trapping. Surface defects might generate a broad range of reactive sites resulting in an exponential decrease of $k_1(\Theta)$ with hydroxyl coverage. Step edge defects have been observed previously in atomic force microscope (AFM) images of the α-Al_2O_3(0001) surface.[15,44] Oxygen vacancy defects may also yield a broad distribution of binding sites. Surface oxygen atom desorption is responsible for the surface reconstruction that occurs on the α-Al_2O_3(0001) surface at high temperature.[12,14,45] However, since the LEED pattern did not show evidence of reconstruction when the surface temperature was kept below 1100 K, the density of oxygen deficiency defects would necessarily be very low.

Evidence against adsorption governed by surface defects is provided by the H_2O TPD spectra from α-Al_2O_3(0001).[29] These

TPD spectra reveal that H_2O desorption occurs from a distribution of hydroxyl sites with different desorption energies ranging from 23 to 41 kcal/mol.[29] However, adsorption into these hydroxyl sites is random and independent of the hydroxyl coverage and hydroxyl binding energy.[29] Consequently, the changes in sticking coefficient with hydroxyl coverage cannot be directly related to the sequential filling of defect sites with progressively decreasing binding energies. This lack of correlation between sticking coefficient and hydroxyl site energy argues against a surface defect explanation.

Alternatively, surface relaxation may account for the strong dependence of the H_2O sticking coefficient on the hydroxyl coverage. On the dehydroxylated α-Al_2O_3(0001) surface, the topmost aluminum layer is relaxed towards the oxygen second layer by ~65% relative to the observed bulk spacing.[16,46] Upon hydroxylation, an aluminum atom may expand toward the oxygen atom of the newly formed hydroxyl group. This expansion may perturb the surrounding Al_2O_3 lattice and cause the additional hydroxylation of neighboring aluminum atoms to be much less favorable.

The coverage-dependent $k_1(\Theta)$ adsorption rate constant may also be associated with repulsive interactions. According to recent calculations,[43] the Al-O-Al*(H_2O) precursor may be H_2O adsorbed on an Al atom on the topmost layer of the α-Al_2O_3(0001) surface. This Al-O-Al*(H_2O) precursor may create a dipole directed toward the surface. Likewise, the AlOH* hydroxyl groups should also produce a dipole directed toward the surface. Dipole−dipole repulsions between the Al-O-Al*(H_2O) precursors and surface hydroxyl groups may cause an increase in the adsorption activation energy versus hydroxyl coverage. These possible repulsions may produce the exponential drop in $k_1(\Theta)$ with hydroxyl coverage. Dipole−dipole repulsive interactions have been invoked previously to account for coverage-dependent adsorption on oxide surfaces.[27,28,47]

In addition, surface trapping may explain the coverage-dependent adsorption rate constant, $k_1(\Theta)$. H_2O molecules that encounter a hydroxyl group on the α-Al_2O_3(0001) surface may partially donate a proton to the surface hydroxyl group to form a strongly bonded $OH^-\cdots{}^+H_2O$-Al surface species. This interaction is observed for α-Al_2O_3 particles in liquid H_2O, and the isoelectric point for α-Al_2O_3 occurs at pH = 9.[48] This $OH^-\cdots{}^+H_2O$-Al surface species may trap H_2O molecules and prevent them from forming surface hydroxyl groups. Consequently, the reactive sticking coefficient for H_2O dissociative adsorption would decrease with increasing hydroxyl coverage.

The pressure-dependent hydroxyl coverage observed at constant H_2O exposure (Figure 9) may result from a H_2O-molecule-catalyzed hydroxylation process.[43] Alternatively, the pressure dependence may result from a collision-induced dissociation mechanism.[42] In this case, collisions between the Al-O-Al*(H_2O) precursor on the surface and any gas phase species may promote hydroxylation. H_2O adsorption experiments performed at constant H_2O pressure but with various pressures of a different gas such as N_2 or Ar may help differentiate between these two processes.

(C) Saturation Hydroxyl Coverage on α-Al_2O_3(0001). The saturation hydroxyl coverage may yield information about the structure of the α-Al_2O_3(0001) surface. Recent experimental[16] and theoretical[46] studies indicate that the dehydroxylated α-Al_2O_3(0001) surface is terminated by aluminum atoms. Figure 6 shows that the hydroxyl coverage saturates at $\Theta_{OH} = 0.5 \times 10^{15}$ OH groups/cm^2 after H_2O exposures $>10^{10}$ langmuir at 300 K. The concentration of aluminum atoms in the topmost atomic layer on α-Al_2O_3(0001) is 0.51×10^{15} atoms/cm^2.[49,50] This close correspondence supports a bonding scheme where the two hydroxyl units produced by dissociative H_2O adsorption occupy all the topmost aluminum atom sites.

According to recent simulations of H_2O dissociative adsorption on the aluminum-terminated surface,[42,43] the OH group from an incoming H_2O molecule is bound to an Al atom in the topmost surface layer and the H atom from the incoming H_2O molecule binds with an O atom in the second oxygen layer to form the second hydroxyl group. On the basis of this reaction scheme, the saturation hydroxyl coverage should equal 2× the aluminum atom surface concentration, or $\Theta_{OH} = 1.0 \times 10^{15}$ OH groups/cm^2. Consequently, the measured saturation hydroxyl coverage of $\Theta_{OH} = 0.5 \times 10^{15}$ OH groups/cm^2 may imply that only 50% of the possible hydroxyl binding sites are occupied at 300 K.

(D) Plasma Hydroxylation. The plot of hydroxyl coverage versus number of plasma cycles in Figure 10 shows no sign of hydroxyl coverage saturation. The measured hydroxyl coverage after one plasma cycle is $\Theta_{OH} = 3.6 \times 10^{15}$ OH groups/cm^2. This coverage is much greater than either the saturation hydroxyl coverage following thermal H_2O exposures or the number of Al sites on the α-Al_2O_3(0001) surface. These plasma hydroxylation results can be explained by surface roughening. The high-energy ions and radicals present in the H_2O plasma may progressively etch the Al_2O_3 surface and increase the surface area and the number of reactive sites.

Surface roughening should also destroy the surface order. In agreement with this expectation, the (1 × 1) hexagonal LEED pattern disappeared following one H_2O plasma treatment. The LEED pattern could only be restored after prolonged thermal annealing at 1100 K. Loss of the LEED pattern for α-Al_2O_3(0001) has also been observed previously following argon ion bombardment at 1-10 keV.[14,45]

Plasmas are commonly used to clean oxide surfaces.[26−28,31] Plasma cleaning very effectively removes carbon contamination. Unfortunately, this plasma treatment may also roughen the α-Al_2O_3(0001) surface. No evidence of plasma roughening was observed during the course of multiple studies of the SiO_2 surface.[26]

(E) H_2O Adsorption on Stratospheric Rocket Exhaust Particles. The H_2O adsorption measurements performed in this work can be used to predict the degree of hydroxylation of stratospheric Al_2O_3 particles generated by solid rocket motors. On the basis of aerosol falling speed data,[51] a typical Al_2O_3 particle will have a stratospheric lifetime of ~10^7 s. Given a H_2O pressure of ~10^{-4} Torr in the stratosphere,[52] this lifetime will produce a 10^9 langmuir H_2O exposure and result in a hydroxyl coverage of $\Theta_{OH} \approx 0.3 \times 10^{15}$ OH groups/cm^2. A more detailed calculation including the H_2O exposure in the rocket plume, the change in stratospheric H_2O pressure along the Al_2O_3 particle trajectory, and the pressure-dependent H_2O adsorption kinetics yields $\Theta_{OH} = 0.32 \times 10^{15}$ OH groups/cm^2. Other forms of Al_2O_3, such as γ-Al_2O_3[53] and α-$Al_2O_3(1\bar{1}02)$,[20] react more readily with H_2O than α-Al_2O_3(0001). Consequently, these predictions may underestimate the true hydroxyl coverage of α-Al_2O_3 particles in the stratosphere.

The effect of hydroxyl groups on the chemical reactivity of α-Al_2O_3 surfaces is not clearly understood. No change in fluorine uptake was measured between hydroxylated and dehydroxylated α-Al_2O_3 surfaces reacted with CF_2Cl_2.[8] However, hydroxylation of α-Al_2O_3 decreased the chlorine uptake by 40−50%.[8] Dehydroxylation tends to increase the catalytic properties of γ-Al_2O_3 by exposing Lewis acid (Al^{3+}) and Lewis base (O^{2-}) surface sites.[1] Some catalytic processes, such as

alcohol dehydration on γ-Al_2O_3, are enhanced by the presence of surface hydroxyl groups.[54] Additional studies are needed to clarify the role of hydroxyl groups on the reactivity of α-Al_2O_3 surfaces and the effect of α-Al_2O_3 particles in the stratosphere.

In addition to hydroxyl groups, stratospheric Al_2O_3 particles may be partially covered with physisorbed H_2O. The present investigation did not detect physisorbed H_2O on the α-Al_2O_3(0001) surface because the H_2O coverage measurements were all performed under UHV conditions. Preliminary measurements reveal that the physisorbed H_2O coverage on Al_2O_3 particles in the stratosphere is less than a few tenths of a monolayer.[9] This physisorbed H_2O may be important for heterogeneous reactions such as $ClONO_2 + H_2O \rightarrow HOCl + HNO_3$.

V. Conclusions

The adsorption of H_2O on a single-crystal α-Al_2O_3(0001) surface was studied using laser-induced thermal desorption (LITD) and temperature programmed desorption (TPD) techniques. These α-Al_2O_3(0001) surfaces exhibited a sharp, (1×1) hexagonal LEED pattern after cleaning and annealing to $T = 1100$ K. Isotopic TPD experiments using $H_2{}^{18}O$ indicated that H_2O dissociatively adsorbs on the Al_2O_3 surface. The initial sticking coefficient of H_2O on α-Al_2O_3(0001) at 300 K measured by LITD experiments was $S \approx 10^{-1}$. The H_2O sticking coefficient decreased nearly exponentially with hydroxyl coverage. The hydroxyl coverage saturated at $\Theta_{OH} = 0.5 \times 10^{15}$ OH groups/cm^2 after H_2O exposures $>10^{10}$ langmuir. In addition, the sticking coefficient was pressure-dependent because the hydroxyl coverage resulting from constant H_2O exposures of 9.2×10^7 langmuir increased versus H_2O pressure. A kinetic model was proposed to explain these results. This model could fit all of the experimental data.

H_2O plasma hydroxylation of α-Al_2O_3(0001) yielded a greater hydroxyl coverage of $\Theta_{OH} = 3.6 \times 10^{15}$ OH groups/cm^2 after one plasma cycle. The hydroxyl coverage increased versus the number of plasma cycles and did not reach a saturation level after eight plasma cycles. These results indicate that plasma hydroxylation roughens the α-Al_2O_3(0001) surface. The H_2O adsorption data was used to predict the hydroxyl coverage on stratospheric α-Al_2O_3 rocket exhaust particles. The predictions reveal that α-Al_2O_3 should be partially hydroxylated at a coverage of at least $\Theta_{OH} \approx 0.3 \times 10^{15}$ OH groups/cm^2. This hydroxyl coverage may affect heterogeneous chemical reactions on these α-Al_2O_3 particles.

Acknowledgment. This work was supported by the Air Force Office of Scientific Research by Grant F49620-96-1-0029. C.E.N. gratefully acknowledges the National Science Foundation for an Atmospheric Training Grant. Some of the equipment used in this work was provided by the Office of Naval Research. M.A.T. was supported as a National Science Foundation Young Investigator and a Camille−Dreyfus Teacher Scholar.

References and Notes

(1) Knozinger, H.; Ratnasamy, P. *Catal. Rev. Sci. Eng.* **1978**, *17*, 31.
(2) Verykios, X. E.; Stein, F. P.; Coughlin, R. W. *Catal. Rev. Sci. Eng.* **1980**, *22*, 197.
(3) Potter, A. E. *J. Environ. Sci.* **1978**, *21*, 15.
(4) Cofer, W. R.; Lala, G. G.; Wightman, J. P. *Atmos. Environ.* **1987**, *21*, 1187.
(5) Jackman, C. H.; Considine, D. B.; Fleming, E. L. *J. Geophys. Res.* **1996**, *101*, 12523.
(6) Robinson, G. N.; Freedman, A.; Kolb, C. E.; Worsnop, D. R. *Geophys. Res. Lett.* **1994**, *21*, 377.
(7) Dai, Q.; Robinson, G. N.; Freedman, A. *J. Phys. Chem. B* **1997**, *101*, 4940.
(8) Robinson, G. N.; Dai, Q.; Freedman, A. *J. Phys. Chem. B* **1997**, *101*, 4947.
(9) Molina, M. J.; Molina, L. T.; Zhang, R.; Meads, R. F.; Spencer, D. D. *Geophys. Res. Lett.* **1997**, *24*, 1619.
(10) Jackman, C. H.; Considine, D. B.; Fleming, E. L. *Geophys. Res. Lett.* **1998**, *25*, 907.
(11) Dill, K. M.; Reed, R. A.; Calia, V. S.; Schulz, R. J. *J. Propul. Power* **1989**, *6*, 668.
(12) Chang, C. C. *J. Appl. Phys.* **1968**, *39*, 5570.
(13) Chang, C. C. *J. Vac. Sci. Technol.* **1971**, *8*, 500.
(14) French, T. M.; Somorjai, G. A. *J. Phys. Chem.* **1970**, *74*, 2489.
(15) Beitel, G.; Markert, K.; Wiechers, J.; Hrbek, J.; Behm, R. J. Characterization of Single-Crystal α-Al_2O_3(0001) and (11-20) Surfaces and Ag/Al_2O_3 Model Catalysts by Atomic Force Microscopy; In *Adsorption on Ordered Surfaces of Ionic Solids and Thin Films*; Umbach, E., Freund, H. J., Eds.; Springer-Verlag: Berlin, 1993; no. 33, Springer series in surface sciences.
(16) Ahn, J.; Rabalais, J. W. *Surf. Sci.* **1997**, *388*, 121.
(17) Morterra, C.; Ghiotti, G.; Garrone, E.; Boccuzzi, F. *J. Chem. Soc., Faraday Trans.* **1976**, *72*, 2722.
(18) Hendriksen, B. A.; Pearce, D. R.; Rudham, R. *J. Catal.* **1972**, *24*, 82.
(19) Rossi, P. F.; Oliveri, G.; Bassoll, M. *J. Chem. Soc., Faraday Trans.* **1994**, *90*, 363.
(20) Schildbach, M. A.; Hamza, A. V. *Surf. Sci.* **1993**, *282*, 306.
(21) Brand, J. L.; George, S. M. *Surf. Sci.* **1986**, *167*, 341.
(22) George, S. M. Laser-Induced Thermal Desorption; In *Investigations of Surfaces and Interfaces*; Rossiter, B. W., Baetzold, R. C., Eds.; John Wiley & Sons, Inc.: New York, 1993; Vol. 2.
(23) Hall, R. B. *J. Phys. Chem.* **1987**, *91*, 1007.
(24) Redhead, P. A. *Vacuum* **1962**, *12*, 203.
(25) Miller, J. B.; Siddiqui, H. R.; Gates, S. M.; Russel, J. N., Jr.; Yates, J. T., Jr.; Tully, J. C.; Cardillo, M. J. *J. Chem. Phys.* **1987**, *87*, 6725.
(26) Sneh, O.; George, S. M. *J. Phys. Chem.* **1995**, *99*, 4639.
(27) Arthur, D. A.; Meixner, D. L.; Boudart, M.; George, S. M. *J. Chem. Phys.* **1991**, *95*, 8521.
(28) Meixner, D. L.; Arthur, D. A.; George, S. M. *Surf. Sci.* **1992**, *261*, 141.
(29) Nelson, C. E.; Elam, J. W.; Cameron, M. A.; Tolbert, M. A.; George, S. M. *Surf. Sci.* **1998**, in press.
(30) Sneh, O.; George, S. M. *J. Vac. Sci. Technol., A* **1995**, *13*, 493.
(31) Poppa, H.; Moorhead, D.; Heinemann, K. *Thin Solid Films* **1985**, *128*, 251.
(32) Gautier, M.; Renaud, G.; Van, L. P.; Villette, B.; Pollak, M.; Thromat, N.; Jollet, F.; Duraud, J. P. *J. Am. Ceram. Soc.* **1994**, *77*, 323.
(33) Brown, D. E.; George, S. M.; Huang, C.; Wong, E. K. L.; Rider, K. B.; Smith, R. S.; Kay, B. D. *J. Phys. Chem.* **1996**, *100*, 4988.
(34) Berland, B. S.; Brown, D. E.; Tolbert, M. A.; George, S. M. *Geophys. Res. Lett.* **1995**, *22*, 3493.
(35) Haynes, D. R.; Tro, N. J.; George, S. M. *J. Phys. Chem.* **1992**, *96*, 8502.
(36) Chen, J. G.; Crowell, J. E.; Yates, J. T., Jr. *J. Chem. Phys.* **1986**, *84*, 5906.
(37) Coustet, V.; Jupille, J. *Surf. Sci.* **1994**, *307*−*309*, 1161.
(38) Frederick, B. G.; Apai, G.; Rhodin, T. N. *Surf. Sci.* **1991**, *244*, 67.
(39) Coustet, V.; Jupille, J., *Proceedings of Workshop on Reactivity of Oxide Materials*; Como, Italy, 1996.
(40) Stirniman, M. J.; Huang, C.; Smith, R. S.; Kay, B. D. *J. Chem. Phys.* **1996**, *105*, 1295.
(41) Guo, J.; Ellis, D. E.; Lam, D. J. *Phys. Rev. B* **1992**, *45*, 45.
(42) Blonski, S.; Garofalini, S. H. *J. Phys. Chem.* **1996**, *100*, 2201.
(43) Wittbrodt, J. M.; Hase, W. L.; Schlegel, H. B. *J. Phys. Chem.* **1998**, submitted.
(44) Barrett, R. C.; Quate, C. F. *J. Vac. Sci. Technol., A* **1990**, *8*, 400.
(45) Vam, L. P.; Gautier, M.; Duraud, J. P.; Gillet, F.; Jollet, F. *Surf. Interface Anal.* **1990**, *16*, 214.
(46) Puchin, V. E.; Gale, J. D.; Shluger, A. L.; Kotomin, E. A.; Gunster, J.; Brause, M.; Kempter, V. *Surf. Sci.* **1997**, *370*, 190.
(47) Sneh, O.; Cameron, M. A.; George, S. M. *Surf. Sci.* **1996**, *364*, 61.
(48) Parks, G. A. *Chem. Rev.* **1965**, *65*, 177.
(49) Causa, M.; Dovesi, R.; Pisani, C.; Roetti, C. *Surf. Sci.* **1989**, *215*, 271.
(50) Thompson, P.; Cox, D. E.; Hastings, J. B. *J. Appl. Crystallogr.* **1987**, *20*, 79.
(51) Kasten, F. *J. Appl. Meteorol.* **1968**, *7*, 944.
(52) Brasseur, G.; Solomon, S. *Aeronomy of the Middle Atmosphere*; D. Reidel Publishing: Dordrecht, Holland, 1997; p 445.
(53) Dillon, A. C.; Ott, A. W.; Way, J. D.; George, S. M. *Surf. Sci.* **1994**, *322*, 230.
(54) Gates, B. C. *Catalytic Chemistry*; John Wiley & Sons: New York, 1992; p 371.